

A Highly Sensitive Amperometric Aptamer Biosensor for Adenosine Triphosphate Detection on a 64 Channel Gold Multielectrode Array

Changtong Wu, Andreas Offenhäusser, and Dirk Mayer*

Herein, an electrochemical aptamer biosensor based on a gold multielectrode array is reported for the detection of adenosine triphosphate (ATP), which is an important neurotransmitter in the central nervous system. The aptasensor possesses 64 individually addressable microelectrodes with a diameter of 24 μm , which is distributed over an area of 1 mm^2 . The electrodes are modified with an ATP-specific aptamer, which is labeled with a ferrocene redox probe. It is demonstrated that the used chip fabrication and cleaning process generate microelectrode channels with similar electrochemical responses and electroactive surface areas. The immobilization of the aptamer on gold microelectrodes is optimized and the receptor density is determined to be $(1.0 \pm 0.44) \times 10^{13}$ molecules cm^{-2} . Concentration-dependent alternating current voltammetry measurements exhibit a limit of detection of 0.30×10^{-9} M and a sensitivity of 2.4 nA logC. Furthermore, the sensor shows a high selectivity over analogous molecules and reproducible detection results in artificial cerebrospinal fluid. The sensor array is used to detect ATP via several channels of the same chip, showing high signal redundancy. A label-free electrochemical, multichannel ATP aptasensor is demonstrated with high selectivity and sub-nanomolar sensitivity, which may be conducive to record this neurotransmitter in neuronal cell-culture systems.

1. Introduction

Adenosine triphosphate (ATP) is the major carrier of chemical energy in living cells, and it plays an important role in regulation


cellular metabolism and biochemical pathways in cell physiology. In particular, ATP has been reported to act as neurotransmitter in the central nervous system.^[1] In 1959, Holton demonstrated the release of ATP on antidromic stimulation of sensory nerve fibers in the skin of rabbit ears, which represented the first evidence for ATP to possess neurotransmitter functions.^[2] Furthermore, Ginsborg and Hirst studied the action of adenosine on neuromuscular transmission from the rat phrenic nerve.^[3] In 1978, a technique was developed to monitor ATP release from rat brain synaptosomes by elevated extracellular K^+ and Ca^{2+} signals.^[4] Later it was suggested that ATP could act as a fast excitatory synaptic transmitter by two groups in 1992.^[5,6] Researchers successfully recorded excitatory synaptic potentials and currents evoked by ATP from coeliac ganglion neurons. With regard to these results, the authors concluded that ATP is an excitatory neurotransmitter in neuron synapses. In the same year, Edwards reported a study to prove neurotransmitter

functions of ATP in the central nervous system by blocking the synaptic current through ATP receptor-blocker, suramin, and the desensitizing ATP receptor-agonist α, β -methylene-ATP.^[7,8] Meanwhile, increasing evidences showed that a deficient ATP release is related to many neuronal dysfunctions, such as brain injuries, strokes,^[9] Parkinson's diseases,^[10] and Alzheimer's diseases.^[11] Given the important biological functions of ATP in various cell systems, detection of ATP in precise and accurate manner is of fundamental importance for in vitro and in vivo investigations of signal transmission in nervous cell systems.

Until now, numerous publications have been reported on ATP detection.^[12–14] The most popular method for ATP detection is via bioluminescence using the ATP-dependent luciferase–luciferin reaction.^[15] However, as the luciferase is not stable in solution, a solid substrate is required and the enzyme activity decreases as well. Alternatively, an aptamer-based ATP binding assay has attracted great interest due to its high specificity and sensitivity.^[16,17] DNA aptamers are single-stranded oligonucleotides with a defined sequence that are artificially selected from random sequence nucleic acid libraries through systematic evolution of ligands with exponential enrichment (SELEX), which can be used to bind various targets with high affinity and

C. Wu, Prof. A. Offenhäusser, Dr. D. Mayer
Institute of Complex Systems (ICS-8)
Bioelectronics
Forschungszentrum Jülich GmbH
52425 Jülich, Germany
E-mail: dirk.mayer@fz-juelich.de

C. Wu, Prof. A. Offenhäusser
Faculty of Mathematics, Computer Science and Natural Sciences
RWTH Aachen University
52062 Aachen, Germany

 The ORCID identification number(s) for the author(s) of this article can be found under <https://doi.org/10.1002/pssa.201900925>.

© 2020 The Authors. Published by WILEY-VCH Verlag GmbH & Co. KGaA, Weinheim. This is an open access article under the terms of the Creative Commons Attribution License, which permits use, distribution and reproduction in any medium, provided the original work is properly cited.

DOI: 10.1002/pssa.201900925

specificity.^[18] The target can be small molecules, drugs, proteins, and cancer cells or viruses. Compared with traditional molecule recognition interactions like antibody–antigen binding, aptamers can provide many advantages such as simplicity of in vitro synthesis, easy labeling, high stability, and high sensitivity.^[19–21] Consequently, aptamers are still emerging for the development of biosensors because the conformational changes induced by target binding can be transduced into optical,^[22] electrochemical,^[23,24] and luminescent signal.^[25] The ATP-binding DNA aptamer (ABA) with a dissociation constant of 6×10^{-6} M was selected by David E. Huizenga and Jack W. Szostak in 1995. It has a stem-bulge-stem structure, which consists of two Watson–Crick helices and two G-quartets, forming a pocket in which the ATP ligand binds.^[26,27]

Due to the high sensitivity and label-free nature of electrochemical detection methods, these techniques possess much potential also for the detection of neurotransmitters. For example, fast scan cyclic voltammetry (CV) has been utilized for the quantification of electroactive neurotransmitters such as dopamine,^[28] adenosine,^[29] and serotonin.^[30] However, considering that some neurotransmitters are nonelectroactive such as ATP, a redox probe-related transducer is certainly required. Implementing redox-tagged aptamers into amperometric E-AB sensors represents a promising approach for the detection of these nonelectroactive small molecules. Although many works have been reported on fabricating E-AB sensor for ATP detection, most of them focused on macroelectrodes.^[24,31] In this work, we used a multielectrode array (MEA) of microelectrodes for the detection of ATP, as the narrowed electrode size can enhance the signal-to-noise ratio in principle, improve the mass transport to the sensor, facilitate spatial resolution of chemical signals, and provide redundant sensor signals. The results in the following parts demonstrated that our aptamer sensor is sensitive and selective towards the analyte ATP.

2. Chemicals and Methods

2.1. Reagents

The ATP aptamer with the sequence 5'-Ferrocene-(CH₂)₆-ACC TGG GGG AGT ATT GCG GAG GAA GGT-(CH₂)₆-SH-3' was purchased from FRIZ Biochem (Neuried, Germany). The aptamer was received as lyophilized powders and stored at -20°C before any usage. The stock solution was prepared by diluting the aptamer powder with 1× TE (Tris-EDTA) buffer (10×10^{-3} M Tris, 1×10^{-3} M EDTA, pH 8.0). The aptamer concentration was determined by UV–vis spectroscopy at 260 nm wavelength. 6-Mercapto-1-hexanol (MCH) and tris-(2-carbo-zyethyl) phosphine hydrochloride (TCEP) were purchased from Sigma-Aldrich (Sigma-Aldrich Chemie GmbH, Munich, Germany) and used without further purification. Guanosine 5'-triphosphate sodium salt hydrate (GTP), cytidine 5'-triphosphate disodium salt (CTP), thymidine 5'-triphosphate sodium salt (TTP), and uridine 5'-triphosphate tris salt (UTP) were used for the selectivity tests. Phosphate-buffered saline (PBS) buffer (10×10^{-3} M PBS, 200×10^{-3} M NaCl, 15×10^{-3} M KCl, pH 7.40) was used as electrochemistry buffer. Tris-HCl buffer (10×10^{-3} M Tris, 1×10^{-3} M EDTA, and pH 7.40) was utilized in the chronocoulometry (CC) measurements to determine

aptamer density. All aqueous solutions were prepared by using ultrapure water ($18.2 \text{ M}\Omega \text{ cm}$; Milli-Q, Millipore). All the measurements were recorded at room temperature.

2.2. Preparation and the Cleaning of Gold MEA

The gold MEA was fabricated in the cleanroom of the Helmholtz Nanoelectronic Facility (HNF), Forschungszentrum Jülich. Each MEA chip has a size of $(24 \times 24) \text{ mm}^2$ and the electrode array is located in the central sensor area with the size of $(1.4 \times 1.4) \text{ mm}^2$ possessing 64 equidistant gold microelectrodes. Each of the microelectrodes has a diameter of $24 \mu\text{m}$ (Figure 1). Borosilicate wafers were used as substrates and cleaned by acetone/isopropanol. After drying in an argon stream, 10 nm titanium was deposited on the wafer as adhesion layer. Then a 200 nm gold layer was deposited via electron beam evaporation on the titanium layer. Finally, an ONONO stacks ($\text{TiO}_2/\text{SiO}_2/\text{Si}_3\text{N}_4/\text{SiO}_2/\text{Si}_3\text{N}_4/\text{SiO}_2$) was deposited on the entire wafer as passivation layer. Contact pads and the actual microelectrode were opened by optical lithography and reactive ion etching (Univex 400, Leybold GmbH, Cologne, Germany). LOR3b and AZ nLOF 2020 (MicroChemicals GmbH, Ulm, Germany) were used as resists. A glass ring with 15 mm diameter was glued on the chip with a thin layer of polydimethylsiloxane (PDMS) (silicon elastomer and the curing agent in a ratio of 10:1, cross-linking bake at 120°C for 1 h) to define a liquid cell for electrochemical measurements.

Before any usage, the newly prepared gold MEAs were first cleaned by ultrasonication in acetone and isopropanol for 5 min to remove fabrication residues. Then an oxygen plasma treatment (0.5 mPa, and 3 min; Pico Plasma System, Diener Electronic GmbH, Ebhausen, Germany) was conducted to ensure that the chips were thoroughly cleaned. Afterward the chips were immersed in ethanol for 15 min to reduce the formed gold oxides. Finally, an electrochemical cleaning in 50×10^{-3} M

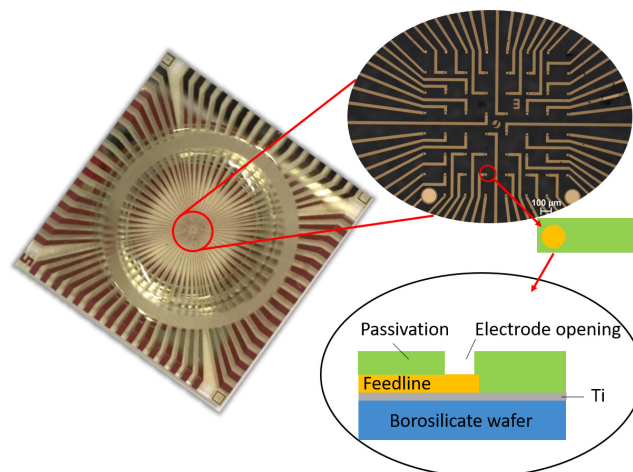


Figure 1. A $(24 \times 24) \text{ mm}^2$ MEA chip containing 64 gold microelectrodes with a distance of $200 \mu\text{m}$ in between. The sensor area was $(1.4 \times 1.4) \text{ mm}^2$ and a glass ring ($17 \text{ mm} \times 5 \text{ mm}$) defined the on-chip electrochemical cell. The magnification shows the central sensor part of the chip with the electrode array, scale bar: $100 \mu\text{m}$. The scheme shows an individual microelectrode in the top and cross sectional side view (bottom).

sulfuric acid was performed by scanning CV between 0 and 1.35 V (Ag/AgCl) at a scan rate of 1 V s^{-1} for 20 cycles.

2.3. Determination of Electrochemical Surface Area and Aptamer Surface Density

The electrochemical surface area (ESA) was obtained by running gold oxidation/reduction cycles via CV scans. First, the potential was cycled 2 times between 0 and 1.35 V (Ag/AgCl) in $50 \times 10^{-3} \text{ M H}_2\text{SO}_4$ at a scan rate of 0.1 V s^{-1} . The surface area was determined by integrating the current peak of the gold oxide reduction from the obtained CV curves. The ESA was obtained from the ratio between the charge of the gold oxide reduction of the studied microelectrode ($Q_{\text{Au/oxide}}$) and standard reference charge for polycrystalline Au.^[32] Based on the literature, the following equation was used to determine ESA of gold electrode. $\text{ESA} = Q_{\text{Au/oxide}}/386$ ($\mu\text{C cm}^{-2}$), where $Q_{\text{Au/oxide}}$ is the reduction peak area.

The aptamer surface density was determined by CC measurements.^[33,34] These experiments were executed in $10 \times 10^{-3} \text{ M Tris-HCl}$ buffer ($10 \times 10^{-3} \text{ M Tris}$, $1 \times 10^{-3} \text{ M EDTA}$, pH 7.40) by performing a potential step from 0 to -0.7 V without and with addition of $10 \times 10^{-3} \text{ M hexaammineruthenium (III) chloride (RuHex)}$. The absolute charge corresponding to surface-confined aptamer (Q_{ss}) can be acquired by calculating the difference between the intercept of linearly fitted plot in the present and absent of RuHex (Figure 2B). The aptamer surface density can be calculated according to following equation

$$\Gamma_{\text{ss}} = (Q_{\text{ss}} N_A / n F A m) (z / m) \quad (1)$$

where N_A is the Avogadro's number, n is the number of electrons in the reaction ($n = 3$), F is the Faraday constant (C mol^{-1}), A is the ESA of gold electrode (cm^2), z is the charge of the redox molecule ($z = 3$), and m is the number of the nucleotides in the aptamer sequence.

2.4. Preparation of ATP Aptamer Sensor and the Electrochemical Measurements

Before any modification, SH-labeled ATP aptamer was pre-treated with $10 \times 10^{-3} \text{ M TCEP}$ for 1 h to reduce the disulfide

bond between the aptamer molecules. Then the aptamer solution with a high concentration of sodium salt was added to the gold electrode and incubated for 16 h overnight at room temperature. A self-assembly aptamer monolayer formed through SH–Au bonds established between the gold surface and thiolate aptamers. Furthermore, $1 \times 10^{-3} \text{ M MCH}$ ethanol solution was used to prevent the unspecific binding of solution born agents and to block those surface sites that were uncovered by aptamers. Then the respective gold electrodes were rinsed with ethanol and $10 \times 10^{-3} \text{ M PBS}$ buffer ($10 \times 10^{-3} \text{ M PBS}$, $200 \times 10^{-3} \text{ M NaCl}$, $15 \times 10^{-3} \text{ M KCl}$, pH 7.40) for 3 times, respectively. The prepared sensor was stored in $10 \times 10^{-3} \text{ M PBS}$ buffer at room temperature before any measurements.

For the detection measurements, alternating current voltammetry (ACV) was utilized as a reliable method to record the target response because it eliminates contributions from the electrode charging from the recorded signals. The measurements were performed on an Autolab potentiostat instrument (PGSTAT302 (Eco Chemie, The Netherlands) with NOVA software) utilizing a three electrode configuration containing a gold working electrode (either macroelectrode or MEA-based microelectrode), an Ag/AgCl reference electrode, and a counter electrode (Pt wire). All potentials mentioned in this publication are quoted with respect to the Ag/AgCl reference potential. The current was measured over potential range from -0.2 to 0.8 V with an ACV amplitude of 5 mV and a frequency of 10 Hz . The electrochemical impedance spectroscopy (EIS) measurement was performed in $5 \times 10^{-3} \text{ M ferri/ferrocyanide (1:1)}$ solution in a $10 \times 10^{-3} \text{ M PBS}$ buffer (pH 7.40) as supporting electrolyte. The impedance was collected in a frequency range from 0.1 Hz to 10 kHz with an amplitude of 10 mV root mean square.

2.5. Test Assays in Diluted Human Serum and Artificial Cerebrospinal Fluid

To challenge the sensor function by relevant test samples, we performed recovery experiments in 100-fold diluted human serum (dHS) mixed with $10 \times 10^{-3} \text{ M PBS}$ buffer (pH 7.40) containing $1 \times 10^{-9} \text{ M ATP}$. Furthermore, we performed additional tests in artificial cerebrospinal fluid (aCSF), which contains according

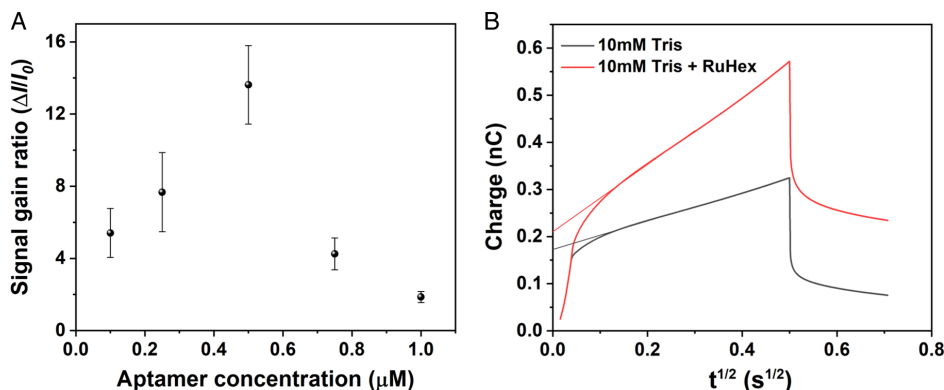


Figure 2. A) Aptamer concentration optimization by comparing the signal gain for different concentrations of 0.1, 0.25, 0.5, 0.75, and $1 \times 10^{-6} \text{ M}$ aptamer. The signal gain is $\Delta I = I_{\text{target}} - I_0$, where I_0 represents the background without any target. B) Determination of the surface density by chronocoulometric measurements in $10 \times 10^{-3} \text{ M Tris}$ buffer and $50 \times 10^{-3} \text{ M RuHex}$.

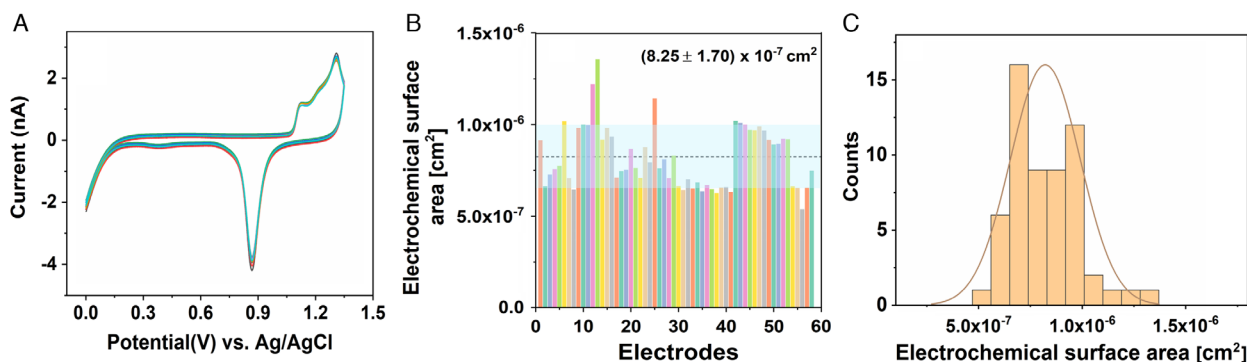


Figure 3. A) Cyclic voltammograms of seven electrodes of the same MEA chip, which were scanned in 50×10^{-3} M H_2SO_4 at a scan rate of 0.1 V s^{-1} with the potential range from 0 to 1.35 V to extract the gold oxide reduction peak. B) The ESA of 58 individual electrodes of the same chip. The black dashed line represents the averaged ESA and the blue window represent the standard deviation. C) The histogram of the ESA corresponds to part (B). The value in the graph indicates the averaged electroactive surface area extracted from fitting the histogram with a Gaussian function.

to the literature approximately 0.3% plasma proteins (mainly albumin).^[35,36] Therefore, aCSF tests containing 45 mg dL^{-1} human serum albumin have been performed in addition as real sample assay. The protein was dissolved in 150×10^{-3} M NaCl, 3.0×10^{-3} M KCl, 1.4×10^{-3} M $\text{CaCl}_2 \cdot 2\text{H}_2\text{O}$, 1×10^{-3} M NaH_2PO_4 , and 0.8×10^{-3} M $\text{MgCl}_2 \cdot 6\text{H}_2\text{O}$ in Milli-Q water. It is noteworthy that concentration of serum proteins is relatively low in most relevant neuronal samples such as aCSF or in vitro culture media (for instance, NEUROBASAL Medium).

3. Results and Discussion

3.1. Electrochemical Characterization of the MEA

At the beginning of the sensor fabrication, the microelectrodes of the multielectrode array were carefully cleaned and the electroactive surface area was determined. A clean electrode surface is critical to facilitate a reproducible electrode aptamer self-assembled monolayer formation. This is true in particular for cleanroom fabricated microelectrodes because residuals of resists or other agents utilized during chip processing can strongly affect the ESA. To estimate the quality and to determine the ESA of the gold MEA, we recorded 2 CV cycles in 50×10^{-3} M H_2SO_4 between 0 and 1.35 V with a scan rate of 0.1 V s^{-1} for several individual microelectrodes of the same chip. Seven representative electrodes were selected which show very similar voltammograms with a sharp reduction peak for each electrode at 0.87 V. However, determining the ESA showed that a certain distribution of the electrode areas existed presumably due to inhomogeneity during the fabrication and cleaning processes. The averaged ESA determined from 58 electrodes of the same MEA was $(8.25 \pm 1.70) \times 10^{-7} \text{ cm}^2$, which is much smaller than the geometrical area value of $4.52 \times 10^{-6} \text{ cm}^2$, which is attributed to the partial passivation of the electrode surfaces by residues. The distribution of the ESA is relatively narrow, but still can influence the performance of the sensor. Therefore, a determination of the ESA seems inevitable to facilitate the determination of quantitative analyte concentrations. This can be achieved by two strategies. First, some electrodes are selected for further sensor applications among all electrodes that possess a similar ESA

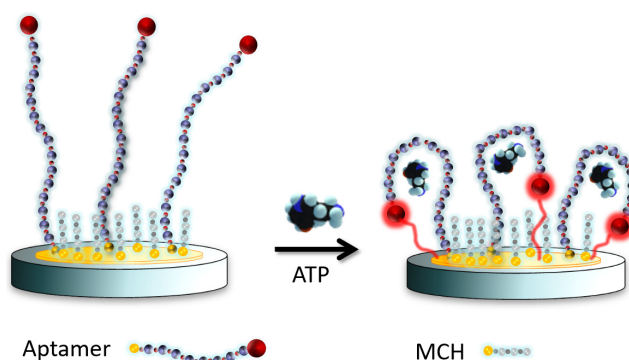


Figure 4. The schematic illustration of the working principle of the amperometric E-AB sensor for ATP detection on a gold MEA. The binding of the ATP analyte causes a change in the aptamer conformation by which the Fc redox probe approaches the electrode surface and enhances the charge transfer.

(see Figure 3A). In the second approach, the obtained sensor signal is corrected by the deviation of the surface area, which has to be determined before, provided that electrode area and sensor signal are directly correlated to each other. Which strategy is used depends on the respective analytical task.

3.2. Working Principle and Characterization of Aptamer Receptor Layer Assembly

The ATP aptamer receptors used in the scope of this work were labeled with a $-\text{SH}$ group at the 3'-terminal end and a ferrocene (Fc) group at the 5'-end (Figure 4). The aptamer was attached on the gold surface via $\text{Au}-\text{SH}$ bonds same as mercaptohexanol, which was used as backfill. In the absence of ATP, the aptamers are unfolded and possess many degrees of freedom to vary its conformation. On average, the Fc redox probes are far away from the electrode surface resulting in small electron transfer efficiency and consequently a low background signal. Upon adding the analyte to the sensor, ATP specifically binds to the aptamers which causes a conformation change. The short

distance between Fc and gold electrode enhances significantly the electron transfer and the current response increases correspondingly. We assume a direct correlation between ATP concentration and current response.

To ensure an optimal sensor sensitivity, the receptor density on electrode surface was optimized by varying the aptamer concentration during its immobilization. Therefore, we determined the redox current change induced by the target binding as a function of the aptamer immobilization concentration. We observed that the E-AB sensor gain strongly depends on the aptamer surface density. For a low aptamer concentrations, the surface density of aptamer receptors is presumably very small and the signal gain remained light. Increasing the concentration first led to increasing and later to decreasing sensor responses. The maximum signal response was observed at 0.5×10^{-6} M with an average signal gain ratio of 13.6 ± 2.2 times (Figure 2A). The lower signal gain for high aptamer concentrations can be explained by electrostatic repulsion between densely packed, negatively charged aptamer molecules that have not enough degree of freedom to fold into the 3D conformation required to bind the analyte.

Furthermore, we determined the resulting surface coverage at this aptamer concentration by chronocoulometric measurements in 10×10^{-3} M Tris buffer (pH 7.40) with 50×10^{-3} M RuHex (Figure 2B). From the difference of the intercepts of the linear fits of the time transients without and with addition of 10×10^{-3} M hexaammineruthenium (III) chloride, the absolute charge corresponding to surface-confined aptamer (Q_{ss}) can be determined. By calculating the reduction charge of RuHex, the number of surface molecules can be obtained according to a common method for ssDNA surface density estimation.^[37] The average surface density is $(1.0 \pm 0.44) \times 10^{13}$ molecules cm^{-2} , which acquired from 45 electrodes on one same MEA. This value is in the same range as observed for macroelectrodes and corresponds to a high aptamer density according to refs. [38–40].

To verify the process of successive immobilization of aptamer and MCH, EIS was used to monitor the stepwise changes in interfacial impedance of the E-AB sensor. For these experiments, a macroscopic gold rod electrode was used because the small diameter of 24 μm of the microelectrode causes very high impedances, which makes EIS experiments very involved. To determine the electrode impedance, the redox couple ferri/ferrocyanide was

added to the analyte solution. The obtained impedance spectra were analyzed by fitting them based on a Randles equivalent circuit comprising a serial electrolyte resistance (R_s), the charge transfer resistance (R_{ct}), a constant phase element (CPE), which improved the fit of the impedance measurements due to inhomogeneity of the electrode surface, and a Warburg impedance accounting for the diffusion of the redox probes to the electrode surface. The charge transfer resistance of the bare electrode was very small with a value at 160 Ω , while it increased to 1.02 k Ω after aptamer immobilization due to the electrostatic repulsion between the negatively charged aptamer molecules and the redox probes ferri/ferrocyanide (Figure 5A). Furthermore, the sample was incubated for 1 h with MCH to reduce the nonspecific binding of analyte molecules and other solution borne substances on the gold surface. We observed a decrease in the resistance to 667 Ω as the MCH has a weaker electrostatic repulsion ability compared with the long aptamer molecules (Figure 5A).^[41] Apparently, the binding of MCH desorbed unspecific bound aptamer molecules from the surface. Finally, an increase in R_{ct} to 782 Ω was observed after addition of 10×10^{-9} M ATP (Figure 5A), which indicates that the negatively charged phosphate groups of ATP electrostatically block the charge transfer between gold electrode and the negative redox probes in solution. Corresponding shifts of the redox peaks and alterations of the peak heights can be found in the CV curves confirming the EIS results (Figure 5B).

3.3. Sensitivity and Selectivity Tests of ATP Aptamer Sensor

Based on the optimal experiment condition, all microelectrodes of the MEA chip were modified with the mixed self-assembled monolayer of aptamer/MCH. The administration of 5×10^{-9} M of ATP caused a clear redox peak at the Nernst potential of Fc in the respective ACV curves recorded for all analyzed microelectrodes, indicating the expected conformational change of the aptamer elicited by ATP binding (Figure 6). The peak heights were very similar except for one electrode (Figure 6E), which showed only approximately 50% signal of the other electrodes. The signal uniformity demonstrates that the electrode responses showed a high redundancy. This finding, however, required that only microelectrode with a similar electroactive surface area was used for the analysis (Figure 3). Also, the electrode that exhibited

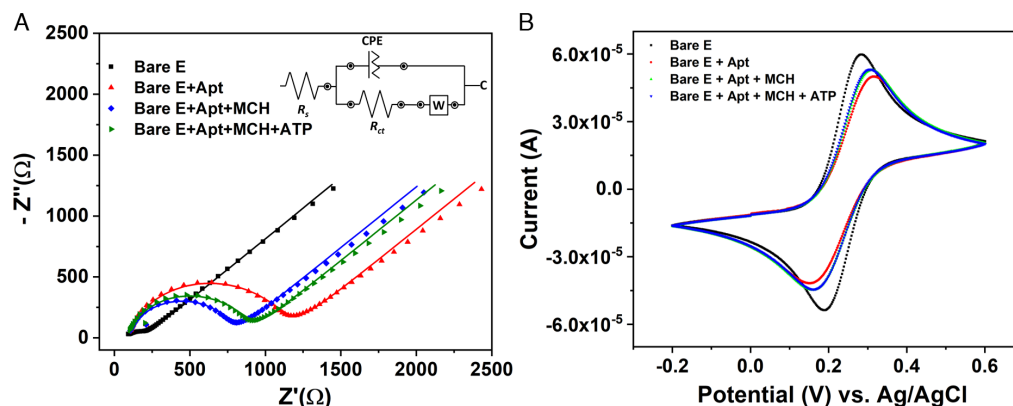


Figure 5. Stepwise characterization of aptamer receptor immobilization by EIS (A) and CV (B) measurements utilizing a macrogold electrode in 5×10^{-3} M ferri/ferrocyanide at pH = 7.40.

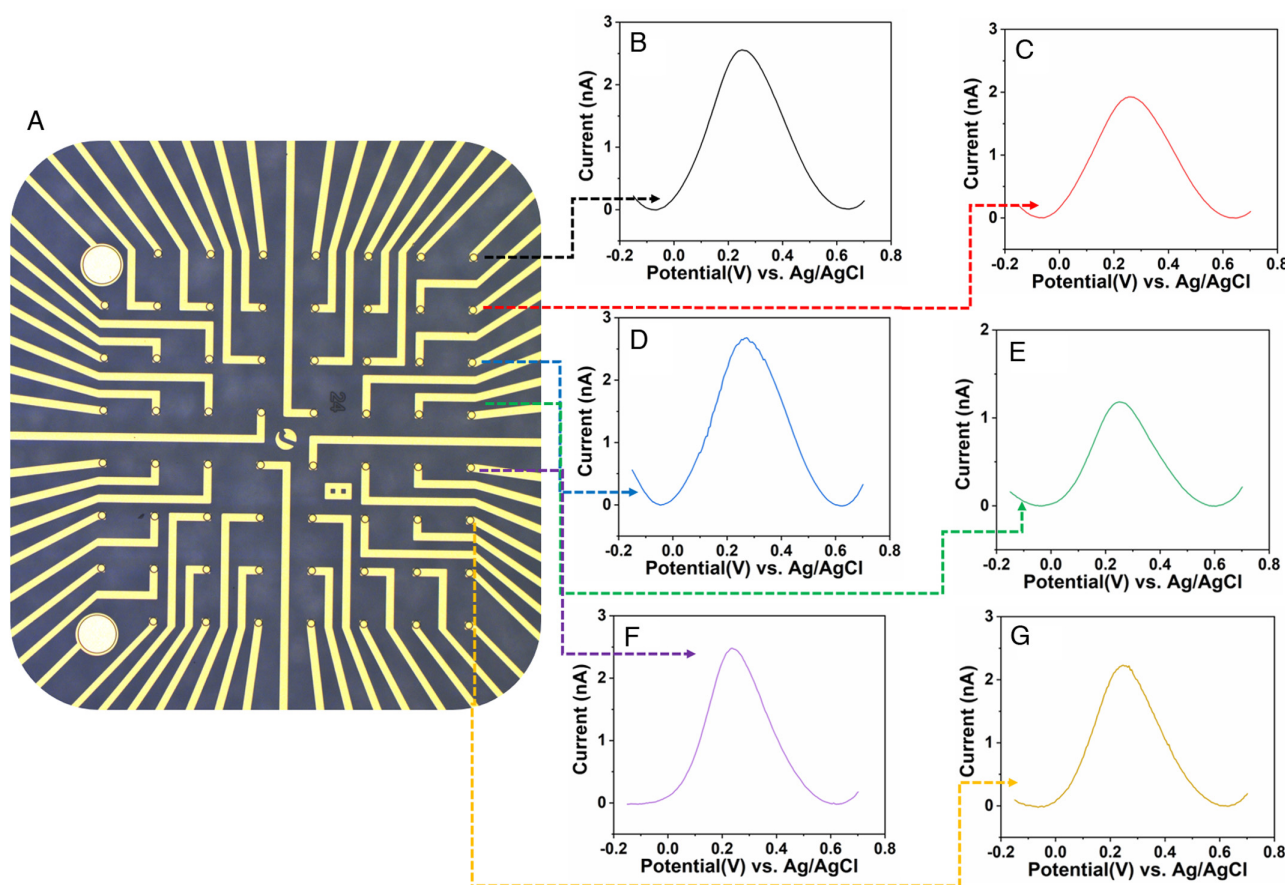


Figure 6. A) Micrograph of a MEA chip showing all 64 microelectrodes and the location of those electrodes that were used for the measurements shown in parts (B–G). B–G) ACV current responses for six adjacent microelectrodes for an ATP concentration of 5×10^{-9} M. Distance between two electrodes was 200 μm .

a deviating peak current height had the same ESA as all other electrodes. This deviation indicates that either the immobilization of the aptamer receptor was not uniform, the electrode degenerated during the experiment, or that there was an inhomogeneous distribution of analyte molecules over the chip. To rule out interfering effects on the receptor layer, it would be advisable to attach an additional redox marker to the binding part of the aptamer, which is not involved in the analyte binding but reports on the number of receptors on the surface. This redox probe would facilitate an in situ evaluation of the integrity of the aptamer film and could be used for drift compensation. Nevertheless, averaging over all recorded channels significantly improves the signal reliability.

The sensitivity of our as-fabricated E-AB sensor was investigated with a series of different concentrations of ATP. Exemplary ACV responses for our ATP aptamer sensor are shown in **Figure 7A** recorded from one microelectrode. As a result of ATP binding, the ACV current increased with rising analyte concentrations. The concentration-dependent current responses from various electrodes with similar ESA were averaged to compile a calibration curve (**Figure 7B**). A linear relationship between redox signals to ATP was obtained in the concentration range from 0.5 to 50×10^{-9} M. The limit of detection (LOD) was

0.30×10^{-9} M according to $S_{\text{dl}} = S_{\text{reag}} + 3\sigma_{\text{reag}}$ with S_{reag} being the averaged signal of the analyte free solution and σ_{reag} representing the standard deviation. The full saturation of the signal was obtained at an ATP concentration of 100×10^{-9} M. The sensitivity of the sensor was derived from the slope of the linear fit in **Figure 7B** to be 2.4 nA logC.

To study the selectivity of our aptamer sensor, the ACV responses of ATP versus its analogues were measured, which were added at a concentration 10 times higher than that of the original analyte. Nevertheless, we observed a distinctly larger current response for ATP compared with its analogues GTP, UTP, CTP, and TTP (**Figure 7C**). This result was confirmed by determining the normalized current responses averaged from three microelectrodes (**Figure 7D**), indicating a preferred binding of ATP over its analogues with very similar chemical structure. Although ATP was added at lower concentration, it nevertheless caused a much higher current response than its analogues, which proves the high selectivity of our microelectrode-based biosensor.

To further test the performance of our aptamer sensor, recovery experiments were performed in 100-fold dHS mixed with 10×10^{-3} M PBS buffer (pH 7.40). 1×10^{-9} M ATP was added to the aptamer sensor, and the ACV signal responses of three different microelectrodes from the same chip were recorded

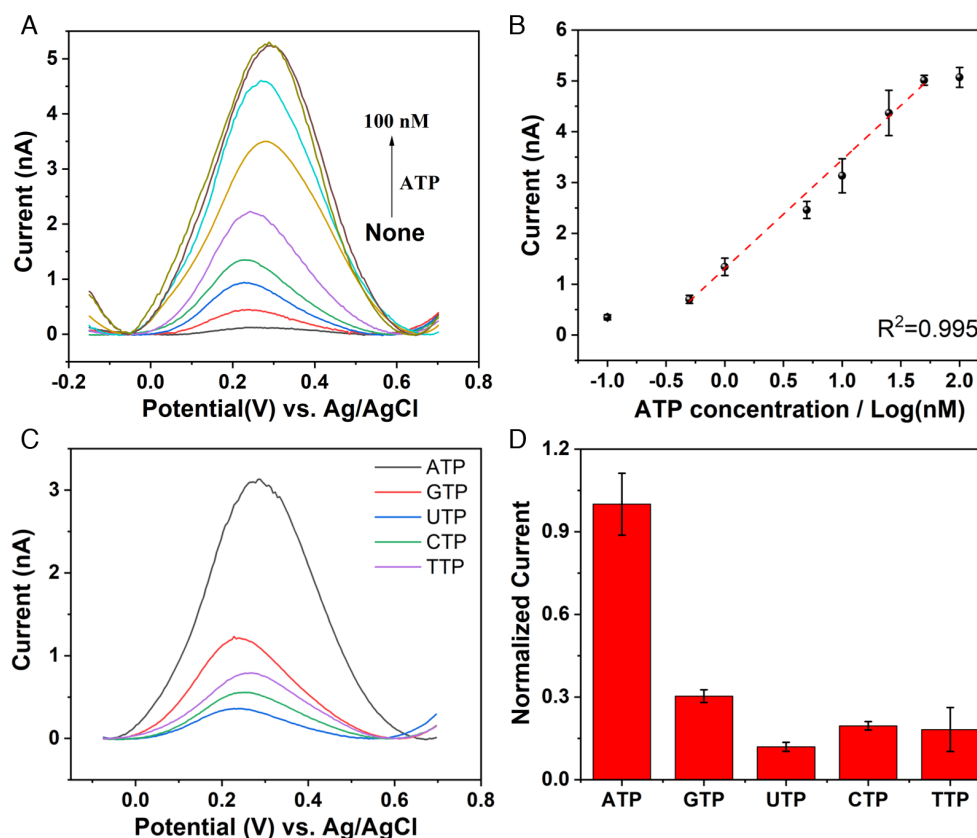


Figure 7. A) ACV current responses of our aptamer sensor with different ATP concentrations from 0 to 100×10^{-9} M. B) Calibration curve of the E-AB sensor by plotting the current response versus the logarithm of ATP concentration. The error bars represent the standard deviation of three electrodes measurement on one chip at each concentration. C) The ACV current response for our E-AB sensor after administration of ATP (100×10^{-9} M) and its analogues GTP, UTP, CTP, and TTP. ATP (all analogues: 1×10^{-6} M). D) The normalized current responses correspond to the results of part (C).

Table 1. The recovery experiments in $100 \times$ dHS and aCSF.

Sample	Electrodes	Added (ATP) [$\times 10^{-9}$ M]	Measured (ATP) [$\times 10^{-9}$ M]	Recovery [%]
dHS	E1	1	0.82	82
dHS	E2	1	0.99	99
dHS	E3	1	1.07	107
aCSF	ME1	1	0.824	82.4

at the same time. According to the linear relationship between ATP concentration and current intensity, the recovery was calculated and shown in **Table 1**. Although the individual electrodes showed a deviation between added and measured ATP concentration of up to 18%, the averaged total signal was $(96 \pm 11.1)\%$ and thus very close to added concentration. The capability of our sensor to obtain a redundant signal output by recording the same signal from several channels improves the reliability of the overall sensor signal. Another important test sample is the cerebrospinal fluid which is present in the brain as well as the spinal cord and is used for the diagnoses of various neurological diseases. We used an aCSF with a similar composition to its native analogous liquor containing 45 mg dL^{-1} human serum albumin.

This test was performed with a different chip. Nevertheless, the recovery of the signal of 1×10^{-9} M ATP in aCSF was 82.4%, although the calibration curve was obtained from different MEAs. These results suggest that our aptamer sensor is able to detect the target with high sensitivity even in relevant complex media such as dHS and aCSF.

4. Conclusions

In conclusion, we have fabricated a selective amperometric E-AB sensor based on a 64 channel gold multielectrode array for the detection of ATP, which is an important neurotransmitter in the central nervous system. Due to the high signal-to-noise ratio and the excellent specificity of the aptamer receptor to its target, the as-fabricated E-AB sensor showed a low LOD value of 0.30×10^{-9} M for ATP detection. Through comparing the ATP signal response versus its analogues such as GTP, UTP, CTP, and TTP, which were added in 10 times excess, the presented sensor exhibited a high selectivity toward ATP. Furthermore, the detection capability in 100-fold dHS and aCSF was investigated. Overall, we believe that our gold MEA-based aptamer sensor can be utilized for neurotransmitter detection with high local resolution. The redundancy of the multichannel sensor improved the signal reliability. This strategy could be pathbreaking for recording

of chemical signals on multiple sites or even the detection of multiple targets such as several neurotransmitters simultaneously on one and the same chip in neuronal cell-culture systems.

Acknowledgements

C.W. gratefully acknowledges the financial support from China Scholarship Council (CSC201608220055). The authors are grateful to Marko Banzet for the fabrication of the MEA chips.

Conflict of Interest

The authors declare no conflict of interest.

Keywords

adenosine triphosphate aptamer sensors, artificial cerebrospinal fluids, microelectrodes, multichannel recording, multielectrode arrays

Received: November 10, 2019

Revised: February 4, 2020

Published online: April 13, 2020

- [1] G. Burnstock, *Trends Pharmacol. Sci.* **2006**, 27, 166.
- [2] P. Holton, *J. Physiol.* **1959**, 145, 494.
- [3] B. L. Ginsborg, G. D. S. Hirst, *J. Physiol.* **1972**, 224, 629.
- [4] T. D. White, *J. Neurochem.* **1978**, 30, 329.
- [5] E. M. Silinsky, V. Gerzanich, S. M. Vanner, *Br. J. Pharmacol.* **1992**, 106, 762.
- [6] R. J. Evans, V. Derkach, A. Surprenant, *Nature* **1992**, 357, 503.
- [7] F. A. Edwards, A. J. Gibb, D. Colquhoun, *Nature* **1992**, 359, 144.
- [8] F. A. Edwards, A. J. Gibb, *FEBS Lett.* **1993**, 325, 86.
- [9] V. Szeto, N. Chen, H. Sun, Z. Feng, *Acta Pharmacol. Sin.* **2018**, 39, 683.
- [10] I. Ferrer, E. Perez, E. Dalfó, M. Barrachina, *Neurosci. Lett.* **2007**, 415, 205.
- [11] I. Cascorbi, C. Flüh, C. Remmler, S. Haenisch, F. Faltraco, M. Grumbt, M. Peters, A. Brenn, D. R. Thal, R. W. Warzok, S. Vogelgesang, *Pharmacogenomics* **2013**, 14, 485.
- [12] Z. Liu, W. Zhang, L. Hu, H. Li, S. Zhu, G. Xu, *Chem. Eur. J.* **2010**, 16, 13356.
- [13] X. Zuo, Y. Xiao, K. W. Plaxco, *J. Am. Chem. Soc.* **2009**, 131, 6944.
- [14] M. Santos-Cancel, L. W. Simpson, J. B. Leach, R. J. White, *ACS Chem. Neurosci.* **2019**, 10, 2070.
- [15] J. A. Cruz-Aguado, Y. Chen, Z. Zhang, N. H. Elowe, M. A. Brook, J. D. Brennan, *J. Am. Chem. Soc.* **2004**, 126, 6878.
- [16] E. J. Cho, J.-W. Lee, A. D. Ellington, *Annu. Rev. Anal. Chem.* **2009**, 2, 241.
- [17] J. Liu, Z. Cao, Y. Lu, *Chem. Rev.* **2009**, 109, 1948.
- [18] M. Mascini, I. Palchetti, S. Tombelli, *Angew. Chem. Int. Ed.* **2012**, 51, 1316.
- [19] W. Li, Z. Nie, X. Xu, Q. Shen, C. Deng, J. Chen, S. Yao, *Talanta* **2009**, 78, 954.
- [20] I. Willner, M. Zayats, *Angew. Chem. Int. Ed.* **2007**, 46, 6408.
- [21] Y. Zhang, G. Figueroa-Miranda, Z. Lyu, C. Zafiu, D. Willbold, A. Offenhäusser, D. Mayer, *Sens. Actuators B* **2019**, 288, 535.
- [22] J. Wang, L. Wang, X. Liu, Z. Liang, S. Song, W. Li, G. Li, C. Fan, *Adv. Mater.* **2007**, 19, 3943.
- [23] L. R. Schoukroun-Barnes, F. C. Macazo, B. Gutierrez, J. Lottermoser, J. Liu, R. J. White, *Annu. Rev. Anal. Chem.* **2016**, 9, 163.
- [24] L. Feng, A. Sivanesan, Z. Lyu, A. Offenhäusser, D. Mayer, *Biosens. Bioelectron.* **2015**, 66, 62.
- [25] J. Wang, Y. Jiang, C. Zhou, X. Fang, *Anal. Chem.* **2005**, 77, 3542.
- [26] D. E. Huizenga, J. W. Szostak, *Biochemistry* **1995**, 34, 656.
- [27] Y.-L. Ying, H.-Y. Wang, T. C. Sutherland, Y.-T. Long, *Small* **2011**, 7, 87.
- [28] J. A. Stamford, Z. L. Kruk, J. Millar, R. M. Wightman, *Neurosci. Lett.* **1984**, 51, 133.
- [29] B. E. Kumara Swamy, B. Jill Venton, *Anal. Chem.* **2006**, 79, 744.
- [30] P. Hashemi, E. C. Dankoski, J. Petrovic, R. B. Keithley, R. M. Wightman, *Anal. Chem.* **2009**, 81, 9462.
- [31] X. Zuo, S. Song, J. Zhang, D. Pan, L. Wang, C. Fan, *J. Am. Chem. Soc.* **2007**, 129, 1042.
- [32] F. Schröper, D. Brüggemann, Y. Mourzina, B. Wolfrum, A. Offenhäusser, D. Mayer, *Electrochim. Acta* **2008**, 53, 6265.
- [33] A. B. Steel, T. M. Herne, M. J. Tarlov, *Anal. Chem.* **1998**, 70, 4670.
- [34] J. Zhang, S. Song, L. Wang, D. Pan, C. Fan, *Nat. Protoc.* **2007**, 2, 2888.
- [35] C. R. Merrill, D. Goldman, S. A. Sedman, M. H. Ebert, *Science* **1981**, 211, 1437LP.
- [36] J. M. Conly, A. R. Ronald, *Am. J. Med.* **1983**, 75, 102.
- [37] R. Lao, S. Song, H. Wu, L. Wang, Z. Zhang, L. He, C. Fan, *Anal. Chem.* **2005**, 77, 6475.
- [38] L. Feng, Z. Lyu, A. Offenhäusser, D. Mayer, *Angew. Chem. Int. Ed.* **2015**, 54, 7693.
- [39] Y. Liang, C. Wu, G. Figueroa-Miranda, A. Offenhäusser, D. Mayer, *Biosens. Bioelectron.* **2019**, 144, 111668.
- [40] R. J. White, N. Phares, A. A. Lubin, Y. Xiao, K. W. Plaxco, *Langmuir* **2008**, 24, 10513.
- [41] G. Figueroa-Miranda, L. Feng, S. C.-C. Shiu, R. M. Dirkwager, Y.-W. Cheung, J. A. Tanner, M. J. Schöning, A. Offenhäusser, D. Mayer, *Sens. Actuators, B* **2018**, 255, 235.